A Pulsed Electromagnetic Eddy Current Method for Detecting Broken Strands of ACSR Conductor in Steel/AL Materials

Yunxing Pu
College of Information Science and Engineering
Northeastern University
Shenyang, Liaoning China
2100673@stu.neu.edu.cn

Jiayue Sun
College of Information Science and Engineering
Northeastern University
Shenyang, Liaoning China
sunjiayue@ise.neu.edu.cn

Qi Xiao
College of Information Science and Engineering
Northeastern University
Shenyang, Liaoning China
1521273922@qq.com

Bowen Zhou
College of Information Science and Engineering
Northeastern University
Shenyang, Liaoning China
zhoubowen@ise.neu.edu.cn

Shuming Liao
College of Information Science and Engineering
Northeastern University
Shenyang, Liaoning China
2100778@stu.neu.edu.cn

***Abstract*—Differ from common cables, aluminum conductor steel reinforced (ACSR) conductors are characterized by internal tensile body of the steel strand and external twisted aluminum strand. Their quality is vital for the safe operation of power grid. However, current researches have been few dedicated studies on broken strands in ACSR conductors. In this paper, a pulsed electromagnetic eddy current (PEMEC) method is proposed to detect the defects of broken strands, in which they occur in steel/AL strands. First, the detection principle is analyzed based on the electromagnetic field propagation properties. Second, this paper describes the damage features from three dimensions: balanced signal, differential signal, and AC magnetic flux density. Basing on the theoretical approach and damage features, this study suggests a PEMEC detection steps to accurately distinguish the broken strand at different positions. Meanwhile, a finite element model is built in COMSOL software, and the PEMEC method' validity is proved, when it is used to detect the varying types, widths and fracture depths of damage in ACSR conductors. In addition, this paper performs a first-order fitting of simulation results to achieve quantification of the damages. Finally, our work is expected to achieve comprehensive detection for broken strands of ACSR conductors.**

Keywords—Aluminum conductor steel reinforced (ACSR), pulsed electromagnetic eddy current method, broken strand, finite element model, damage quantification

I. INTRODUCTION

Composite materials are frequently used in power equipment to improve their physical stability and strength in long-term outdoor operation. High voltage transmission lines (HVTL) are primarily composed of ACSR conductors, which may be subject to damage from various external factors such as acid rain corrosion, chemical pollutant corrosion, lightning, wind vibration, and others [1]. If some weeny damages in HVTL are not discovered in time, they will gradually affect the safe and stable transport of electricity [2]. Hence, regular damage detection is necessary in the daily operation and maintenance process. Currently, commonly used methods for detecting defects in HVTL include visual inspection or drone inspection [3]. However, these methods have limited accuracy in detecting potential defects and are reliant on human labor.

Non-destructive testing (NDT) methods based on electromagnetic principles have unique advantages [4, 5], which have been widely applied in various applications, such as oil and gas pipelines [6] and steel cables [7]. Moreover, excellent detection methods provide a stable dataset environment for subsequent intelligent detection [8, 9]. Pulsed eddy current (PEC) method has gained popularity as a new method in NDT and has shown remarkable results in terms of many fields [10, 11]. This method employs square wave excitation, which can be considered as a combination of multiple frequency components, and overcomes the limitations of conventional eddy current detection, such as the skin effect. Therefore, PEC detection has a greater penetration depth compared to other EC NDT methods.

In the field of damage detection on HVTL, Xia et al. have proposed the eddy current (EC) differential coils in series and a corresponding signal processing circuit to detect the damages of AL strand in ACSR conductors [12, 13]. However, the method is limited to detect the inner damage, due to the limitations of the EC penetration depth. For the detection of ferromagnetic materials, Wang et al. utilized a U-shaped yoke to form a magnetic circuit, which has been shown to be highly effective in detecting full-angle cracks in pipes [14-16]. Similarly, the U-shaped yoke was applied to the detection of damage of steel in ACSR conductors [17-19]. They quantified the assessment of broken strands and loss of metallic area (LMA). However, neither of these methods could achieve the

simultaneous detection of composite materials. To detect the broken steel/AL strands in ACSR conductors, Liao et al. proposed a method using pulsed signals with high penetration capability [20]. They differentiated damage types in both materials based on the responsive pulse voltage peak/time ratio.

In this work, we aimed at proposing a combination of a U-shaped yoke and the PEMEC method to enhance the accuracy of damage detection in ACSR conductors. The pulsed signal's high penetration properties are leveraged to improve the detection depth and sensitivity in both AL/steel strand. In this paper the defect characteristics are analyzed in three dimensions: balanced signal, differential signal, and AC magnetic flux density. Besides, a 2-D finite element model is established to demonstrate the accuracy of PEMEC method under different types, widths and depths of defects.

This paper is organized as follows: Section 2 provides the principle and step of PEMEC method. Section 3 presents the simulation model and the measurement results. Besides, this section quantifies the width and depth of the broken strands and discusses the probe strengths. The conclusions and future works are summarized in Section 4.

II. PEMEC DETECTION PRINCIPLE

A. *The basic theory*

PEMEC is based on the principles of PEC and pulsed magnetic flux leakage (PMFL). The probe consists of three parts shown in Figure 1. The yoke is a flux bar made of high permeability magnetic material, channeling the magnetic flux in the direction of the material. The excitation coil is connected low power stimulating signals to generate magnetic flux. The receiving coils include balanced coil and differential coil.

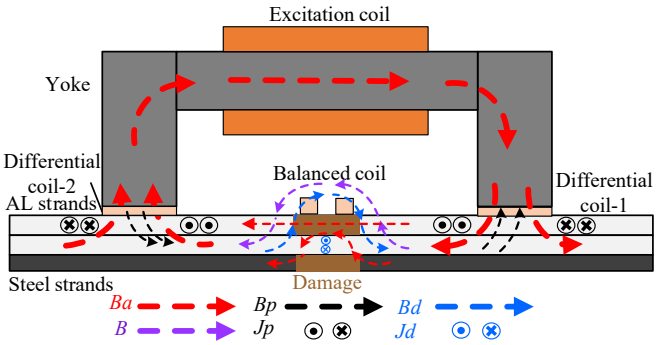

Fig. 1. Principle of PEMEC detection

According to the low frequency electromagnetic field theory, the electromagnetic problems of displacement current and surface charge could be neglected. Thus, the A-ϕ principle is adopted for the solution [14-16].

$$rot\left(\frac{1}{\mu}rot\boldsymbol{A}\right)=\boldsymbol{J}_0-\sigma\left(\frac{\partial\boldsymbol{A}}{\partial t}+grad\phi\right) \tag{1}$$

$$div\left\{-\sigma\left(\frac{\partial\boldsymbol{A}}{\partial t}\right)+grad\phi\right\}=0 \tag{2}$$

where $\boldsymbol{A}$ denotes the magnetic vector, ϕ denotes the electrical scalar, μ denotes the permeability, $\boldsymbol{J}_0$ denotes the source current density, $\boldsymbol{J}_d=\sigma\frac{\partial\boldsymbol{A}}{\partial t}$ denotes the magnetic circuit eddy current near the damage, $\boldsymbol{J}_p=\sigma grad\phi$ is the eddy current under the yoke' poles, and σ denotes the of the conductivity.

Based on Ampere's circuital theorem, the relationship between magnetic flux density and current density could be described by the following equations [14-16].

$$\nabla\times\boldsymbol{B}_a=\mu\boldsymbol{J}_s \tag{3}$$

$$\nabla\times\boldsymbol{B}_p=\mu\boldsymbol{J}_p \tag{4}$$

$$\nabla\times\boldsymbol{B}_d=\mu_0\boldsymbol{J}_d \tag{5}$$

$$\boldsymbol{B}=\boldsymbol{B}_a+\boldsymbol{B}_d+\boldsymbol{B}_p \tag{6}$$

where μ denotes the vacuum permeability, $\boldsymbol{B}_a$ denotes the AC leakage magnetic field, $\boldsymbol{B}_p$ denotes the magnetic field induced by $\boldsymbol{J}_p$, $\boldsymbol{B}_d$ denotes the magnetic field induced by the magnetic circuit eddy current $\boldsymbol{J}_d$, and $\boldsymbol{B}$ denotes the magnetic field superimposed on the AC leakage magnetic field and the eddy current induced magnetic field. The spatial distribution of the magnetic flux density and current density is shown in Figure 1.

In Figure 2, the detailed detecting processes could be divided into two phases: the pulsed phase and the DC phase.

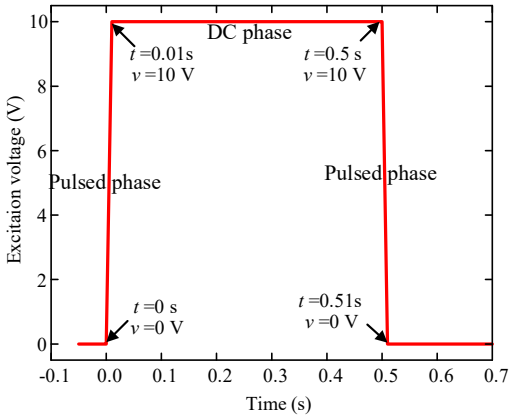

Fig. 2. Time-domain waveform of pulse-excited voltage.

During the pulsed phase, the pulsed signal generates an alternating magnetic field, which passes through the excitation coil and penetrates the composite material along the U-shaped yoke. Firstly, an eddy current field is established near the contact surface, and then in the magnetic circuit. If the ACSR conductors are damaged, it will result in distortions in the axial eddy current field, which could be detected by the receiving coils. Besides, when the steel is damaged, the magnetic line will be refracted at the defective partition interface. Part of the magnetic flux will leak from the ACSR conductors' surface to generate a magnetic leakage field.

When the excitation signal transitions to the DC phase, the eddy current field will disappear. At this time, the probe will detect the damage of steel strands alone for magnetic flux leakage. Therefore, in both phases, AL/steel broken strands are presented differently. With the differential coils under the

magnetic feet and the balanced coil, all signals could be picked up for damaging classification.

B. PEMEC detection step

Based on the magnetic field distribution characteristics and coils arrangement, this paper proposes three defect features: balanced signal, differential signal, and AC magnetic flux density. A PEMEC detection step is proposed, as illustrated in Figure 3.

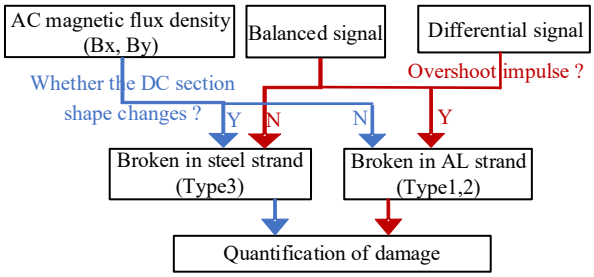

Fig. 3. PEMEC detection step

Due to the different magnetic permeability, electrical conductivity and position of AL/steel strands, the damages show different characteristics in pulsed phase and DC phase. Firstly, the shape of the Bx/By at the observation point provides a direct indication of the damage types. Secondly, the damage position is also located based on the shape of the signal detected by the balanced coil and the differential coil. Finally, the width and depth of the damage is quantified based on these signals. The whole detection process is completed.

III. ANALYSIS OF SIMULATION RESULTS

This section employs simulation calculations to identify and extract the damage features. Building upon the PEMEC method presented above, this section develops a finite element equivalent model to analyze and investigate different damage types, widths and depths in three dimensions. The feasibility and effectiveness of the PEMEC method will be validated.

A. Modelling and Simulation

This paper uses COMSOL Multiphysics software to build an equivalent 2-D simulation model of the ACSR conductors and the probe, as shown in Figure 4.

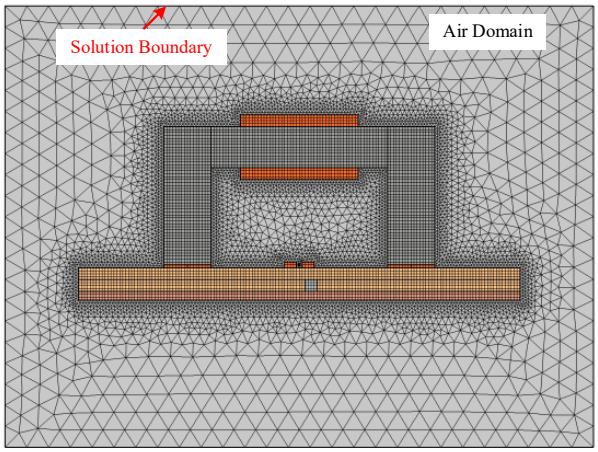

Fig. 4. 2D finite element meshing model

The ACSR conductors in the model comprise of two layers of 4mm-thick AL strands and one layer of 3mm-thick steel strand, with a total length of 150mm. The U-shaped yoke has dimensions of 92mm in length, 47mm in height, 16mm in width, and a pole spacing of 60mm. The excitation coil has an outer diameter of 22mm, an inner diameter of 14mm, and a height of 40mm. The differential flat coils have an outer diameter of 16mm. The balanced coil has an outer diameter of 10mm, an inner diameter of 2mm, and a height of 2mm. The electromagnetic parameters of the model are listed in Table 1.

TABLE I. Electromagnetic parameters of model

Parameters	values
The relative magnetic permeability of steel strands	400
The conductivity of steel strands/(S/m)	5×10^{6}
The relative magnetic permeability of AL strands	1
The conductivity of AL strands /(S/m)	3.774×10^{7}
The relative magnetic permeability of yoke	2000
The conductivity of yoke /(S/m)	0.2
The conductivity of coils/(S/m)	5.998×10^{7}

Notches are placed in the ACSR conductors to simulate damage, as depicted in Figure 5. This paper categorizes the damage into three types: outer damage of AL strand, inner damage of AL strand, and damage of steel strand. The damage widths for each type are set from 2mm-6mm.

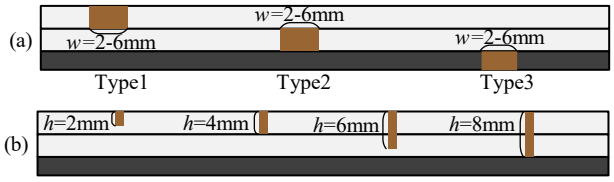

Fig. 5. Distribution of damage in ACSR. (a) Variation of damage width(w) under different types, (b) Different fracture depths

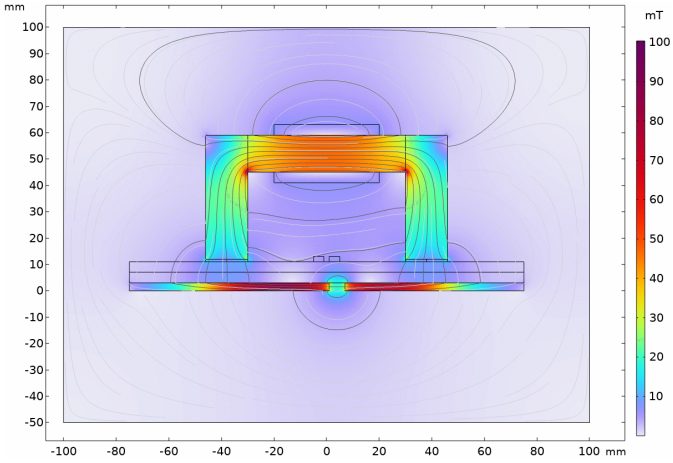

Fig. 6. Magnetic field distribution in DC phase. Unit: mT

Figure 6 displays the magnetic field distribution of the damage of steel strand during the DC phase. The graph clearly shows that the magnetic flux density exhibits an axisymmetric

distribution along the centerline of the yoke. It is evident that the DC magnetic leakage phenomenon is pronounced when the steel strand is damaged.

B. Magnetic flux densities at observation point

With the observation points described in the middle of the magnetic pin line, it is straightforward to compare the magnetic flux density variation for different damage types. As shown in Figure 7, the left portion represents the magnetic flux leakage in the Bx direction, while the right portion represents the magnetic flux leakage in the By direction.

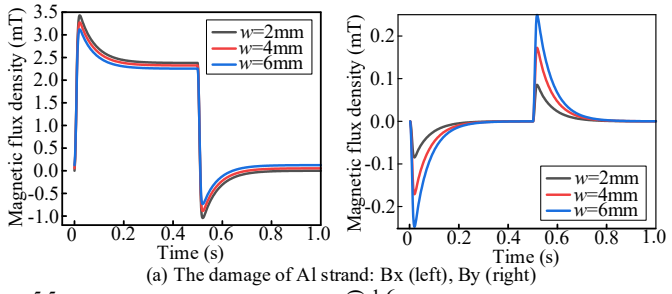

(a) The damage of Al strand: Bx (left), By (right)

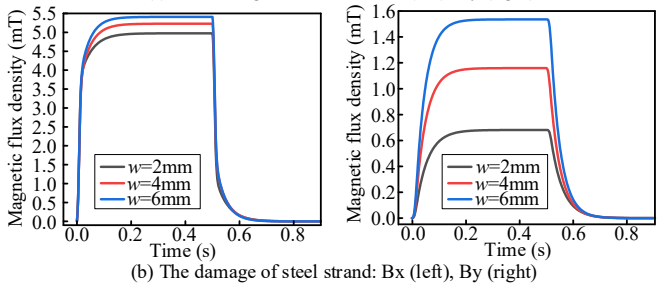

(b) The damage of steel strand: Bx (left), By (right)

Fig. 7. Magnetic flux density of different damage positions

As demonstrated in the figure 7, the damage types of the AL strand and the steel strand are highly distinguishable in both Bx and By directions. This distinctive signal can be captured by magnetically sensitive elements. For the damage detection of AL strand, the magnetic field changes occur during the pulsed phase. However, like the depths of damage, the variation is small, comparing to the normal. Due to the low relative magnetic permeability of AL strand, it couldn't be detected in DC phase. On the other hand, because of the high magnetic permeability, the damage of steel stand means it could be detected during both the pulse phase and the DC phase. Therefore, the damage expression of steel strand is more pronounced in the DC phase.

C. Comparison of detection voltages

Figure 8 depicts the signals of various damage widths for different types and damage depths of steel/AL strands. The left section of the diagram presents all the signals detected by the balanced coil, while the right section displays the signals from the differential coils. Since the signal is symmetric about the y-axis in both positive and negative half-periods, the graph only shows up to 0.3s.

Based on the analysis of the time-domain response voltage of damages, several viewpoints could be made. Specifically, the following summarizes the findings.

- During the pulsed response phase, the detection voltage for damage of AL strand exhibits a conspicuous overshoot impulse. The voltage response crosses the zero point and then returns. In contrast, when steel strand is damaged, the voltage signal doesn't cross zero. Instead, it shows a gradual decline.
- Of the three impulse signals examined (i.e., steel strand damage signal, AL strand damage signal, and reference signal), the steel strand damage signal exhibits antiphase behavior with both the other signals.
- In terms of signal amplitude, the intensity of damage signal in the outer layer is higher than that in the inner layer, and the amplitude increases with the damage width. The buffer time for the balanced signal is significantly smaller than that for the differential signal.

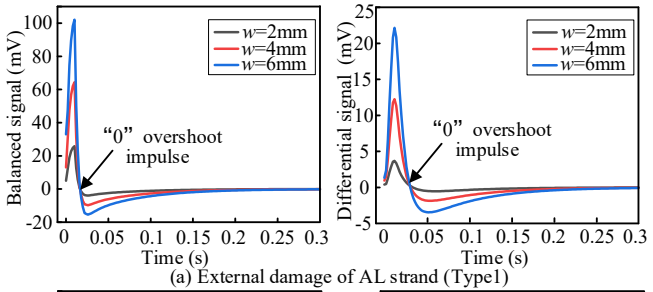

(a) External damage of AL strand (Type1)

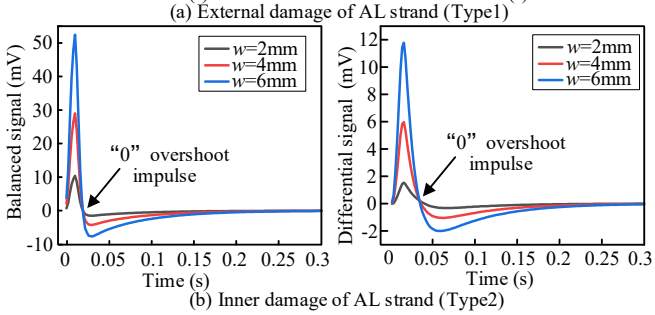

(b) Inner damage of AL strand (Type2)

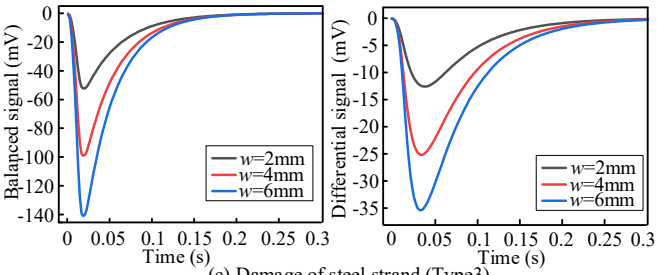

(c) Damage of steel strand (Type3)

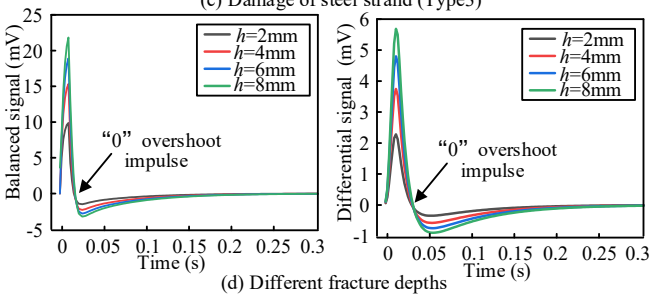

(d) Different fracture depths

Fig. 8. Detection voltages for different damage types

D. Quantification analysis

This subsection presents a further analysis of the simulation results. As previously mentioned, the detection voltage is symmetrical between the positive and negative half-periods

and is processed within 0.3s. For the damage's signals of AL strand, the balanced signal is the algebraic sum of the maximum value and the overshoot minimum value. In contrast, for the steel strand damage signal, the differential signal is the maximum of the algebraic value. The fitting results are presented in Figure 9.

$$Z(d) = \prod_{w=2-6mm} \left\{ \max_{t=0-0.3s}(X), \min_{t=0-0.3s}(X) \right\} \quad (7)$$

where X denotes the function of the original signal composition and Z is the processed data. Γ denotes the linear fit function. w denotes the damage width.

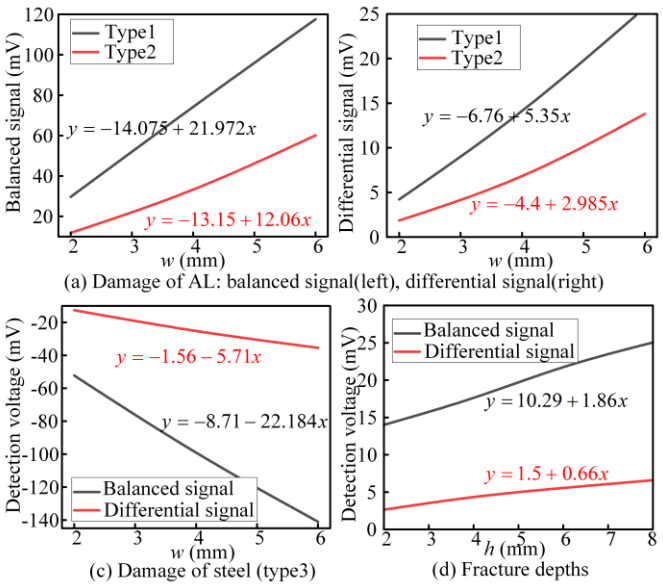

(a) Damage of AL: balanced signal(left), differential signal(right)

(c) Damage of steel (type3)

(d) Fracture depths

Fig. 9. Fitting results

The differential signal and the balanced signal show a linear pattern, suggesting that both damage depths and widths could be characterized numerically with a linear model. Moreover, the changing rate of voltage distinguishes both types of damage. Consequently, the changing rate of voltage amplitude is one of the effective distinguishing features.

It should be noted that the fitting results for AL strand show a negative intercept, which doesn't indicate a reverse voltage change but rather the existence of a minimum detectable voltage. Based on the present simulation and geometric parameters, the minimum of the balanced coil required to detect outer damage of AL strand is estimated to be 0.64mm, while the minimum for inner damage of AL strand is 1.09mm. The minimum of the differential coils required to detect outer damage of AL strand is estimated to be 1.2mm, while the minimum for inner damage of AL strand is 1.48mm.

Besides, to enable comparison, the By direction of magnetic flux density in Figure 7 could be quantified using a linear Hall sensor, such as the WCS138 (±20mT, 8.3mV/Gs, 10Gs = 1mT). The fitting results for the Hall sensor output voltage are shown in Figure 10.

In contrast, the minimum of the linear Hall sensor required to detect outer damage of AL strand is estimated to be 0.01mm, while the minimum for inner damage of AL strand is 0.99mm. When detecting strand damage, the width of the damage could be straightforwardly quantified based on the voltage and the magnetic flux density in the DC phase.

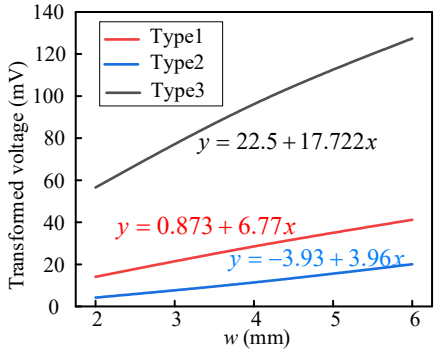

Fig. 10 Transformed voltage from By

IV. CONCLUSION

For the lack of effective methods for damages detection of ACSR conductors strand, this paper proposes a PEMEC method. Using COMSOL Multiphysics software to build and simulate a finite element model, the authors develop the damage characterizations from three dimensions: differential signal, balanced signal and magnetic flux density. On this basis, this paper explores the variation in detection characteristics at different locations, widths and depths of damage. An in-depth analysis of the results suggests the following conclusions.

1) The PEMEC method effectively detects damage to steel/AL strands through voltage peaks, that could quantify the width and depth of the damage. The coexistence of multiple damages requires further exploration.

2) Compared to direct EC method of single frequency or PEC method, the PEMEC method expands the detection range, enhances differentiation of steel and AL damage, and improves detection capabilities from three dimensions.

ACKNOWLEDGMENT

This work was supported by the National Key R&D Program of China (2022YFB4100802) and National Natural Science Foundation of China (U1908217、U22B20115).

REFERENCES

[1] Y. Goda, S. Yokoyama, S. Watanabe, T. Kawano and S. Kanda, "Melting and breaking characteristics of OPGW strands by lightning," IEEE Transactions on Power Delivery, vol. 19, no. 4, pp. 1734-1739, Oct. 2004, doi: 10.1109/TPWRD.2004.832410.

[2] Azevedo, C. R. F., and T. Cescon. "Failure analysis of aluminum cable steel reinforced (ACSR) conductor of the transmission line crossing the Parana River." Engineering Failure Analysis 9.6 (2002): 645-664.

[3] S. Ashidate, S. Murashima, and N. Fujii, "Development of a helicopter-mounted eye-safe laser radar system for distance measurement between power transmission lines and nearby trees," IEEE Transactions on Power Delivery, vol. 17, no. 2, pp. 644-648, Apr. 2002, doi: 10.1109/61.997953.

[4] H. Song, Q. Xiao, G. Wang, J. Zhang, and W. Hu, "A composite approach of electromagnetic acoustic transducer and eddy current for inner and outer corrosion defects detection," IEEE Transactions on Instrumentation and Measurement, vol. 72, pp. 1-11, 2023, Art no. 6001211, doi: 10.1109/TIM.2023.3238689.

[5] J. Feng, Q. Li, Q. Xiao, and G. Wang, “A method of Rayleigh wave combined with coil spatial pulse compression technique for crack defects detection.” IEEE Transactions on Instrumentation and Measurement. vol. 72, pp. 1-11, Feb. 2023.

[6] G. Wang, Y.-T. Li, and Q. Xiao. “Finite-element study of remote field eddy current method for inner diameter and outer diameter pipe defects classification.” INSIGHT. vol. 65. no. 3, pp. 1-7, 2023.

[7] X. Liu, J. Xiao, B. Wu, and C. He. “A novel sensor to measure the biased pulse magnetic response in steel stay cable for the detection of surface and internal flaws.” Sensors and Actuators A: Physical, vol. 269, pp. 218-226, Jan. 2018.

[8] X. Ni, D. Yang, H. Zhang, F. Qu and J. Qin. “Time-Series Transfer Learning: An Early Stage Imbalance Fault Detection Method Based on Feature Enhancement and Improved Support Vector Data Description.” IEEE Transactions on Industrial Electronics, vol. 70, no. 8, pp. 8488-8498, Aug. 2023, doi: 10.1109/TIE.2022.3229351.

[9] D. Yang, J. Qin, Y. Pang and T. Huang. “A Novel Double-Stacked Autoencoder for Power Transformers DGA Signals with an Imbalanced Data Structure.” IEEE Transactions on Industrial Electronics, vol. 69, no. 2, pp. 1977-1987, Feb. 2022, doi: 10.1109/TIE.2021.3059543.

[10] Q. Xiao, J. Feng, Z. Xu, and H. Zhang, “Receiver signal analysis on geometry and excitation parameters of remote field eddy current probe," IEEE Transactions on Industrial Electronics, vol. 69, no. 3, pp. 3088-3098, Mar. 2022, doi: 10.1109/TIE.2021.3063958.

[11] Q. Xiao, J. Feng, S. Lu, S. Liu, and H. Zhang, “Accurate identification for 3-D position of hybrid defects in ferromagnetic pipe using external remote field eddy current testing," IEEE Transactions on Magnetics, vol. 58, no. 3, pp. 1-10, Mar. 2022. doi: 10.1109/TMAG.2022.3141233.

[12] Y. Xia, X. Jiang, Z. Zhang, J. Hu and C. Sun. “Detecting broken strands in transmission line—Part 1: Design of a smart eddy current transducer carried by inspection robot.” International Transactions on Electrical Energy Systems, vol. 23, no.8, pp. 1409-1422, Jul. 2013.

[13] Y. Xia, X. Jiang, Z. Zhang, J. Hu, and C. Sun. “Detecting broken strands in transmission line−Part 2: Quantitative identification based on S-transform and SVM.” International Transactions on Electrical Energy Systems, vol. 23, no. 8, pp. 1423-1439, Jun. 2012.

[14] G. Wang, Q. Xiao, M. Guo, and J. Yang, “Optimal frequency of ac magnetic flux leakage testing for detecting defect size and orientation in thick steel plates.” IEEE Transactions on Magnetics, vol. 57, no. 9, pp. 1-8, Sep. 2021, Art no. 6200708, doi: 10.1109/TMAG.2021.3095593.

[15] G. Wang, Q. Xiao, Z. Gao, *et al.*, “Multifrequency AC Magnetic Flux Leakage Testing for the Detection of Surface and Backside Defects in Thick Steel Plates,” IEEE Magnetics Letters, vol. 13, pp. 1-5, 2022, Art no. 8102105, doi: 10.1109/LMAG.2022.3142717.

[16] J. Feng, Q. Xiao, S. Lu, and H. Zhang, “A double remote magnetic field synthesis method for reducing high-speed MFL signal distortion caused by velocity effect,” IEEE Transactions on Industrial Electronics, doi: 10.1109/TIE.2023.3239857. (Early access)

[17] F. Lv, P. Zhang, Z. Tang, Y. Yue, and K. Yang. “A guided wave transducer with sprayed magnetostrictive powder coating for monitoring of aluminum conductor steel-reinforced cables.” Sensors, vol. 19, no. 7, pp. 1550, Mar. 2019.

[18] C. Zhou, C. Wei, and W. Wang, “A new detection method based on magnetic leakage theory and BP neural network for broken steel strands in ACSR conductor.” IEEE Sensors Journal, vol. 22, no. 20, pp. 19620-19634, Oct. 2022, doi: 10.1109/JSEN.2022.3202253.

[19] Y. I. Brahim, J. Bellemare, G. Rousseau, N. Pouliot, D. Ménard, and F. Sirois. “Ultrasensitive lightweight magnetic probe for non-destructive inspection of high-voltage overhead lines.” NDT & E International, vol. 134, 102781, Mar. 2023.

[20] C. Liao, Y. Yi, T. Chen, C. Cai, Z. Deng, X. Song, and C. Lv. “Detecting broken strands in transmission lines based on pulsed eddy current.” Metals, vol. 12, no. 6, 1014, Jun. 2022.